HEFAT2014
10th International Conference on Heat Transfer, Fluid Mechanics and Thermodynamics
14 – 16 July 2014
Orlando, Florida

A MECHANISM OF POLYMER INDUCED DRAG REDUCTION IN TURBULENT PIPE FLOW

Zadrazil I.* and Markides C.N.
*Author for correspondence
Department of Chemical Engineering,
Imperial College London,
London, SW7 2AZ,
United Kingdom,
E-mail: i.zadrazil06@imperial.ac.uk

ABSTRACT

Polymer induced drag reduction in turbulent pipe flow was investigated using a non-intrusive laser based diagnostic technique, namely Particle Image Velocimetry (PIV). The drag reduction was measured in a pressure-driven flow facility, in a horizontal pipe of inner diameter 25.3 mm at Reynolds numbers ranging from 35 000 to 210 000. Three high-molecular-weight polymers (polyethylene oxide 2×10^6 – 8×10^6 Da) at concentrations in the range of 5 – 250 wppm were used. The results, obtained from the PIV measurements, show that the drag reduction scales with the magnitude of the normalized streamwise and spanwise rms velocity fluctuations in the flow. This scaling seems to universal, and is independent of the Reynolds number and in some cases also independent of the distance from the wall where the velocity fluctuations are considered. Furthermore, the instantaneous PIV observations indicate that as the level of drag reduction increases, the flow in the pipe is separated into a low-momentum flow region near the pipe wall and a high-momentum flow region in the turbulent core. Based on these findings a new mechanism of polymeric drag reduction is proposed in this paper.

INTRODUCTION

High molecular weight polymers or surfactants dissolved at very low concentrations in a solvent lead to a significant reduction of mechanical drag in turbulent flow when compared to the equivalent flow of the pure solvent. This phenomenon, known as drag reduction (DR) and reported for the first time by Toms [1] and Mysels [2], is of great industrial relevance, e.g., in the oil-and-gas industry (pipeline systems or hydraulic fracturing), agriculture (field irrigation) and civil engineering (firefighting, plane refueling).

The phenomenon of drag reduction has been extensively studied in the past, however, previous studies were limited to the gross-flow characterization, i.e., the effect of drag reducers on the friction factor at a given Reynolds number *Re* [3,4]. Although highly valuable, such studies were unable to provide a detailed insight into the mechanistic turbulence-polymer interactions at the microscopic level.

Recently, the utilization of advanced laser-based flow diagnostics techniques, e.g., Laser Doppler Velocimetry and Particle Tracking Velocimetry, for the characterization of drag reducing solutions has provided both quantitative and qualitative results. Liberatore et al. [5] observed that the frequency and the intensity of large scale ejections decreased in the presence of polymer additives. Warholic et al. [6] identified turbulent structures close to the wall which are typical for Newtonian solvents. These structures were characteristic by the ejection of low momentum fluid to the outer velocity-defect region. Such structures were identified as locations of large Reynolds stresses. These structures, however, were absent at high measured levels of drag reduction.

NOMENCLATURE

D	[m]	Inside pipe diameter
DR	[%]	Drag reduction
r	[m]	Pipe radius
Re	[-]	Reynolds number
u'	[m/s]	Streamwise velocity fluctuation
U_{bulk}	[m/s]	Bulk velocity
v'	[m/s]	Spanwise velocity fluctuation
y	[m]	Distance from the wall

Special characters

Δp	[Pa]	Differential pressure
$\bar{u}$	[m/s]	Mean streamwise velocity
$\bar{U}$	[m/s]	Mean velocity
τ	[m^2/s^2]	Reynolds stress
ρ	[kg/m^3]	Density
μ	[Pa s]	Dynamic viscosity

Subscripts

a	Drag reducing additive
N	Normalized variable
rms	Root mean square
s	Solvent

One of the remarkable features of polymer induced drag reduction in turbulent flow is the evolution of Reynolds stresses with increasing drag reduction, which were found to decrease with increasing level of drag reduction [7]. Warholic et al. [8] found almost zero Reynolds stresses for a maximum drag reduction in a channel flow across the entire channel. However, this has not been observed for a pipe flow where the level of Reynolds stress was lowered in the presence of polymer additives but never reached zero values [7,9].

This paper follows on from our previous investigation of drag reducing flows using Particle Image Velocimetry [10] where the presence two distinctive layers within the turbulent flow was uncovered. In the present paper we provide a quantitative characterization of drag reducing flows with a special emphasis on the scaling of important variables that characterize the turbulent flow with the level of drag reduction. In addition, based on our previously published observations, we provide a novel mechanism of polymer induced drag reduction in turbulent flow which is based on the presence of 3D entangled polymer network in the near-wall area.

EXPERIMENTAL METHODS

Linear non-ionic water soluble polymer, namely Polyethylene oxide (PEO), of different molecular weights was used in this work. The molecular weights investigated were 2×10^6; 4×10^6 and 8×10^6 g/mol with corresponding abbreviations PEO2, PEO4 and PEO8, respectively. Concentrations of 5; 10; 25; 50; 75; 125 and 250 wppm (i.e., parts per million by weight) of each of the three polymer molecular weights were prepared and studied. Tap water was used as a solvent.

Drag reduction of fresh polymer solutions was measured using a flow facility set-up in a one-pass flow order. Additionally, a recirculation pump was installed at the end of the test section in order to allow for the investigation of the flow induced polymer mechanical degradation in turbulent pipe flow, see Figure 1. A detailed description of the flow facility can be found in Zadrazil et al. [10], hence, we will provide here only a brief description. The flow facility is composed of a preparation low-speed stirring tank (Tank I), pressurized tank which allows for the liquid to be pneumatically driven through the test section (Tank II), 7.1 m long $D = 25.3$ mm (where D is the test section inside diameter) stainless steel pipe test section, drain tank (Tank III) and a set of measuring instrumentation.

A magneto-inductive flow-meter was used to measure the liquid flow-rate and the Reynolds numbers investigated, based on the flow-rate and viscosity measurements, were Re = 35 000; 70 000; 110 000; 140 000 and 210 000. This gives, together with the three different polymer molecular weights, seven polymer concentrations and three extended experimental runs to investigate flow induced polymer degradation, a total of 122 experimental conditions. The macro-scale Reynolds number is given by:

$$Re = \frac{\rho U_{\text{bulk}} D}{\mu} \qquad (1)$$

where ρ is the density, U_{bulk} the bulk velocity in the test section ($\pi D^2/4$) and μ the dynamic viscosity measured by a commercial rheometer equipped with cone and plate measuring geometry. It should be noted that all the polymer solutions investigated exhibited Newtonian behavior.

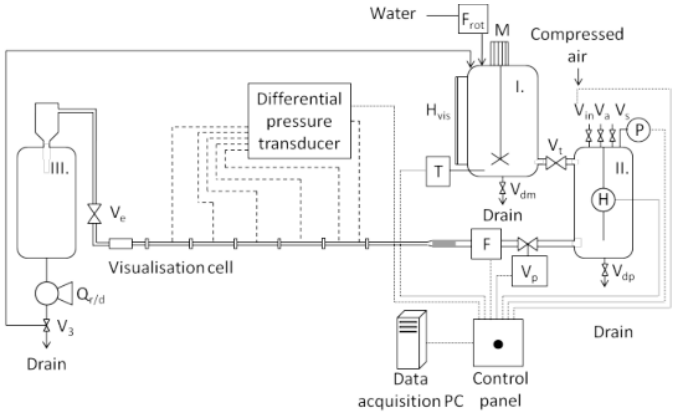

Figure 1 Schematic illustration of the drag reduction flow facility (taken from Ref. [10]).

The level of drag reduction was quantified by means of differential pressure drop Δp measured along the test section by six membrane differential transducers. The reference tap was located at 1.76 m downstream the inlet and the subsequent measurement taps at 1.96; 2.96; 3.96; 4.96; 5.96 and 6.96 m from the inlet. The level of drag reduction was calculated by:

$$DR = \left(\frac{\Delta p_{\text{s}} - \Delta p_{\text{a}}}{\Delta p_{\text{s}}} \right)_{Re=\text{const}} \qquad (2)$$

where the subscripts "s" and "a" stand for the solvent and polymer containing solution, respectively.

The turbulent flow was measured at a distance of 6.11 m from the test section inlet using a non-intrusive laser based technique, namely Particle Image Velocimetry (PIV). A transparent visualization section with the outside flattened and polished was used for the PIV measurements. Such a design minimizes the optical distortion caused by the difference in the refractive indices between the test section material and air. In addition, any remaining optical distortion due to the difference in refractive index between the visualization section material and the visualized liquid was corrected by using a graticule (printed target) correction technique [11]. The uncertainty in the position of individual visualized pixels was 33 μm.

The PIV system compose a double-pulsed frequency doubled Nd:YAG laser (532 nm) and a monochromatic CMOS camera. During the measurements, seeding particles (glass hollow spheres with a mean diameter of 9 – 13 μm) within the flow were illuminated by a laser sheet and the elastically scattered light was recorded by a camera position at 90° to the laser light sheet. The visualized area was 16.0×12.8 mm which with the camera resolution of 1280×1024 yields a spatial

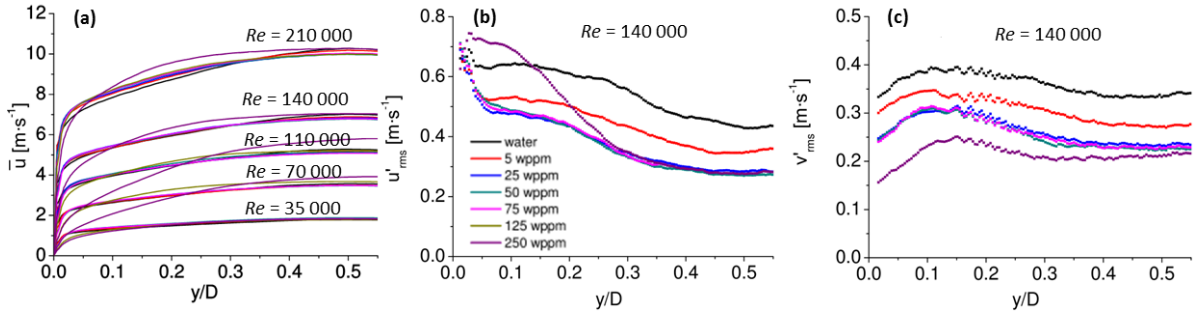

Figure 2 (a) mean streamwise velocity $\bar{u}$ for PEO8, (b) rms streamwise velocity fluctuations u'_{rms} for PEO8 at *Re* = 140 000 and (c) rms spanwise velocity fluctuations v'_{rms} for PEO8 at *Re* = 140 000; all shown as a function of normalized distance from the wall *y*/*D*.

resolution of 25 μm. During each measurement a set of 500 images was taken at a frequency of 100 Hz.

The raw images were initially corrected for optical distortions and pre-processed using an algorithm that subtracted a sliding minimum over three images. The images, containing elastically scattered light from the seeding particles, were then processed using a commercial PIV algorithm utilizing a cross-correlation function employing a multi-pass technique. A total of three cross-correlation passes was used: (i) PIV interrogation window of 32×32 pixels with 25% overlap of the adjacent areas, and (ii) and (iii) 16×16 pixels with 50% overlap. Finally, the velocity vector maps were post-processed using a median filter in order to remove and replace any spurious vectors.

RESULTS

Figure 2 shows profiles (as a funtion of nornalized distnace from the pipe wall, *y*/*D*) of the mean stremwise velocity $\bar{u}$ for water, PEO2, PEO4 and PEO8 at different *Re*, as well as an example of streamwise u'_{rms} and spanwise v'_{rms} velocity fluctuation rms profiles for PEO8 at *Re* = 140 000. The maximum level of drag reduction observed in this work was 72%. The mean streamwise velocity profiles, Fig. 2(a), were obtained by time averaging the 500 instantaneous velocity vector images followed by the spatial averaging along the *x*-axis (streamwise direction). The $\bar{u}$ profiles follow a typical logarithmic turbulent flow trend with a peak value at the centreline *y*/*D* = 0.5. A deviation from the $\bar{u}=f(y/D)$ trends can be observed for the highest concentrations of PEO8, and the highest measured level of drag reduction for given flow conditions, which can be explained by a some degree of the flow laminarization.

The velocity profiles, such as those in Figure 2(a), have been used for the estimation of uncertainties during the PIV measurements. An integration of the velocity profiles yields the

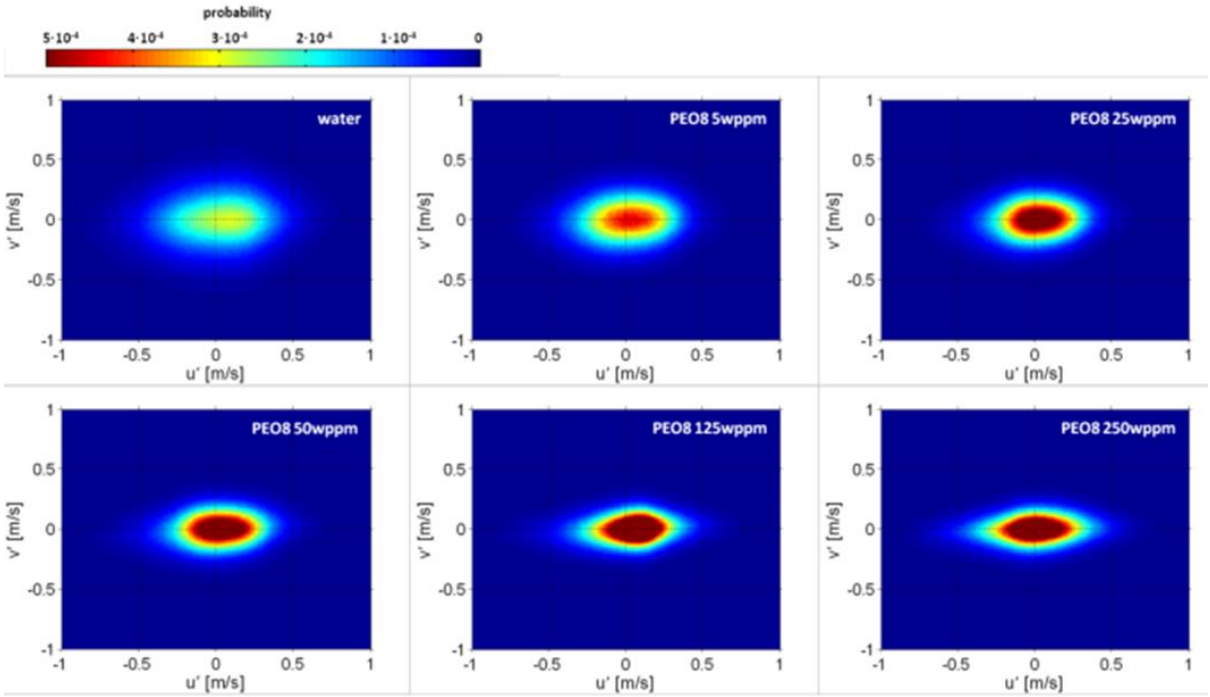

Figure 3 Joint probability function of the streamwise and spanwise velocity fluctuations (u' and v') for PEO8 solutions at *Re* = 70 000.

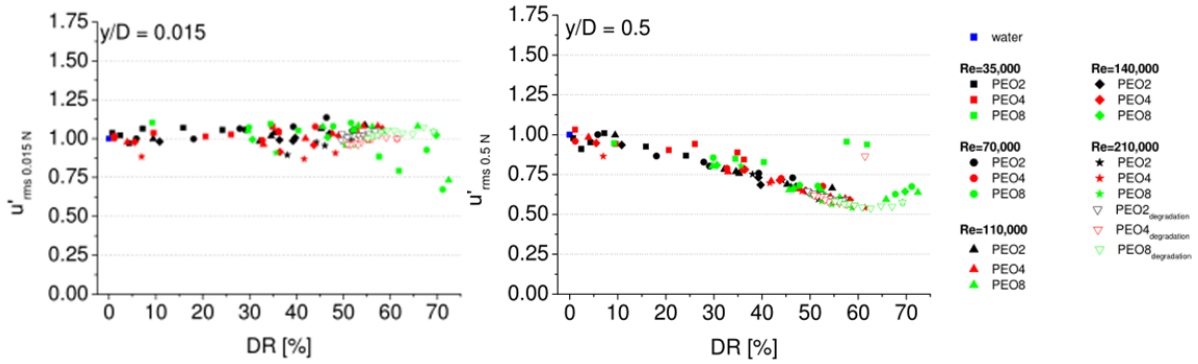

Figure 4 Dependence of normalized rms streamwise velocity fluctuations on the level of measured drag reduction at (a) $y/D = 0.015$ and (b) $y/D = 0.5$.

bulk velocity U_{bulk}:

$$U_{bulk} = \frac{1}{\pi r^2}\int_0^r \bar{U}(y)2\pi(r-y)dy \qquad (3)$$

where r is the pipe radius, y the distance from the wall and $\bar{U}$ the mean velocity at y distance from the wall. Note that $\bar{u}(y)$ and $\bar{U}(y)$ are almost identical since the contribution of the mean spanwise velocity component to the mean velocity is negligible. A comparison of U_{bulk} values to those obtained from the flow-meter showed an average difference of -6.2%.

In general, the intensity of both streamwise and spanwise rms velocity fluctuations increases with increasing Re (results not shown). In the case of u'_{rms} profiles, see Fig. 2(b), the values of u'_{rms} decrease with increasing distance from the wall with a peak value in the inner near-wall region. Contrary, the intensity of spanwise velocity fluctuations, see Fig. 2(c) peaks at $y/D \sim 0.1 - 0.2$. The height of the peak decreases with increasing polymer concentration and corresponding level of drag reduction. Additionally, the peak value is shifted towards the outer velocity-defect region with increasing polymer concentration, which is in agreement with den Toonder et al. [9] and White et al. [12].

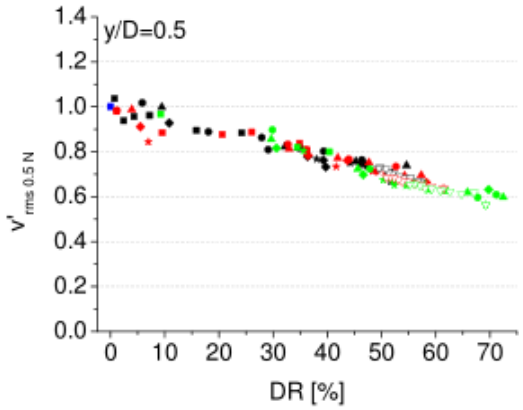

Figure 5 Dependence of normalized rms spanwise velocity fluctuations on the level of drag reduction at $y/D = 0.5$ (i.e., the centreline). The legend for this plot is identical to the one shown in Figure 4.

The joint probability functions (JPF) of streamwise u' and spanwise v' velocity fluctuations for PEO8 at $Re = 70\,000$ is shown in Figure 3. The JPF was constructed from 250 bins and the probability of the occurrence of the velocity fluctuations is shown by the colour-bar. It can be seen that the polymer additives reduce the magnitude of velocity fluctuations the probability is shifted towards zero velocity fluctuation values with increasing polymer concentration. Additionally, the polymer additives reduce the spanwise fluctuation to a higher extent than the streamwise velocity fluctuations and the JPFs become more elliptic with increasing polymer concentration (and consequently the level of drag reduction). This indicates that the polymer additives cause the turbulence to become anisotropic, which is in agreement with Warholic et al. [6] who found that polymer additives reduce the spanwise velocity fluctuations more than the streamwise. The anisotropy of the velocity fluctuations was observed for all polymers studies (i.e., PEO2, PEO4 and PEO8) and over the whole range of Re.

Typically it is difficult to infer the effect of drag reducers on turbulence from various profiles (see Fig. 2). Hence, in this paper, we provide a comparison of normalized turbulence parameters based on:

$$X_{y/D;\mathrm{N}} = \frac{X_{y/D;\mathrm{a}}}{X_{y/D;\mathrm{s}}}_{Re=\mathrm{const.}} \qquad (4)$$

where X represents a turbulent flow variable (e.g., u'_{rms} or v'_{rms}) and the subscripts y/D; "N"; "a" and "s" represent the distance from the wall where the variables were normalized; normalized quantity; polymer additive related variable and water related variable, respectively. The unity value; based on this normalization, represents the normalized variable for the pure Newtonian solvent (i.e., water) independently of Re.

The dependence of normalized rms streamwise velocity fluctuations at $y/D = 0.015$ and 0.5 on the level of measured drag reduction is shown in Figure 4. The first point to be noted is that the data became independent of Re for a given y/D. For the near-wall area ($y/D = 0.015$), the effect of drag reducers is negligible with the exception of the highest levels of drag reduction where a decrease in $u'_{rms\ 0.015;N}$ can be observed. This

decrease is likely to be linked with the shift of the peak u'_{rms} value away from the wall (see Fig. 2(b)). It is interesting that the shift of the u'_{rms} peak value demonstrates itself through the entire pipe cross-section. Indeed, an increase of the normalized rms streamwise velocity fluctuations for the highest levels of drag reduction can be observed even at the centre of the pipe $y/D = 0.5$. Additionally, the relative intensity of the streamwise velocity fluctuations is almost halved for the high levels of drag reduction at the centre of the pipe.

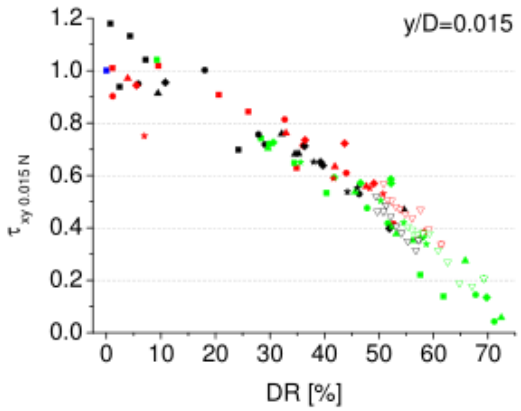

Figure 6 Dependence of normalized Reynolds stress on the level of drag reduction at $y/D = 0.015$ (i.e., near-wall area). The legend for this plot is identical to the one shown in Figure 4.

Similarly to the rms streamwise velocity fluctuations, the normalized rms spanwise velocity fluctuations at $y/D = 0.5$ are shown in Figure 5. Also in this case the normalization produced a universal trend-line, i.e., independent of *Re*, however, the polymer additives decrease the spanwise velocity fluctuation up to the same extent irrespective the y/D with a slope of -0.0053. The results presented indicate that the polymer drag reducing agents modify both the streamwise and spanwise velocity fluctuations over the whole radius of a pipe and that the relative alteration is independent of *Re*.

Finally, Figure 6 shows the dependency of normalized Reynolds stress as a function of drag reduction at $y/D = 0.015$. Remarkably, the normalized Reynolds stress values decreased to close to zero values at the maximum measured drag reduction, independently of the distance from the wall (not shown). Warholic et al. [8] indeed observed almost zero Reynolds stresses across a channel at the maximum drag reduction.

The instantaneous turbulent flow field measurements see Fig. 7, have been already shown and discussed in Zadrazil et al. [10], hence, we will limit here to the description of the main features. In general, the instantaneous measurements of local speed, 2D vorticity, streamwise shear strain rate and velocity fluctuations revealed the presence of low-momentum regions in the vicinity of the wall separated by a shear layer from the high-momentum region around the centreline axis. The position of the interfacial boundary, i.e., the shear layers, scaled with the level of measured drag reduction in a similar fashion to those shown in Figs. 4, 5 and 6. Indeed, as discussed by Zadrazil et al. [10] the thickening of the low-momentum regions with increasing drag reduction resembled the thickening of a buffer layer in the presence of drag reducing additives.

The presence of a region with a discontinuity in the instantaneous velocities which is associated with high values of instantaneous 2D vorticity and low values of instantaneous streamwise strain rate is a significant indication for the

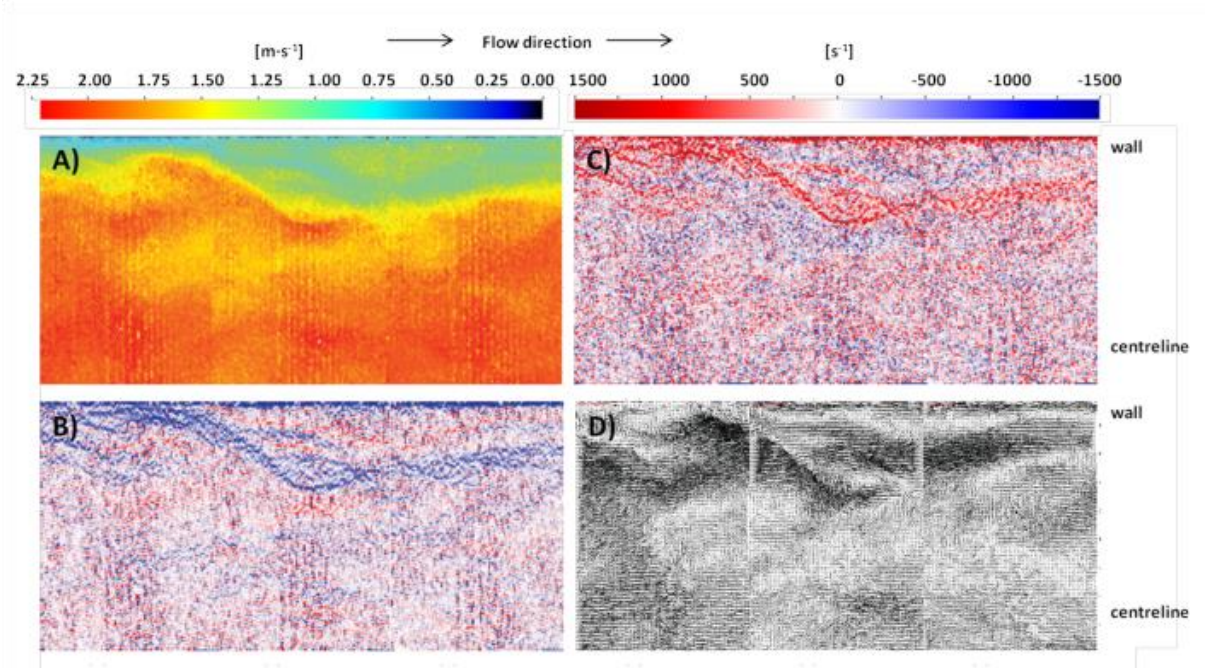

Figure 7 A stitched-together sequence of the instantaneous: (a) local speed, (b) 2D voracity, (c) streamwise shear strain rate and (d) velocity fluctuations (vector) maps, all for PEO8 125 wppm at *Re* = 35 000.

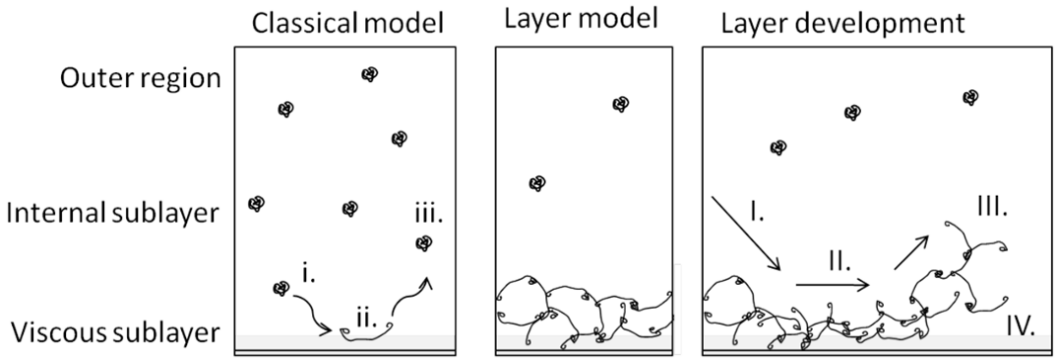

Figure 8 Polymer layer mechanism of drag reduction.

existence of two different flow layers – low momentum layer in the vicinity of the wall and high momentum layer in the velocity-defect region. The very low polymer concentration, well below the critical polymer overlap concentration, employed in drag reducing solutions led to the drag reduction explanations based on the behaviour of individual polymer molecules [13]. Classical drag reduction mechanisms consist of the following polymer-turbulence interactions: (i) the transfer of polymer molecules to the inner near-wall region, (ii) the elongation of polymer molecules in the inner near-wall region and (iii) the relaxation of polymer molecules to random coil conformation in the more quiescent outer velocity-defect region, see Fig. 8(a). The aforementioned dynamics of polymer molecules in turbulent flow would, however, not result in the observed flow separation accompanied by the presence of interfacial shear layers.

In order to explain the new observations, we propose a polymer layer mechanism of drag reduction, see Figure 8(b) and (c). An elongated polymer molecule has significantly lower polymer overlap concentration when compared to a polymer molecule in a random coil conformation. When a polymer molecule elongation takes place in the inner near-wall region, the local polymer dilution character also changes and the possibility of a collision of two or more polymer molecules significantly increases. Additionally, the presence of the wall decreases the freedom of movement of polymer molecules whose can migrate only towards the velocity-defect region. The outcome of such collisions of highly elongated polymers would be a formation of a 3D physically-entangled polymer structure, see Fig. 8(b). Indeed a polymer network structures were observed for PEO solutions subjected to elongation flow in a cross-slot cell [14]. Such a 3D network would not be stationary, but would be affected by the outer velocity-defect region environment as well as by the turbulence generation in the near-wall area. This hypothetical example of the development of such a 3D structure is shown in Fig. 8(c): (I) turbulent flow fluctuations in the far-wall region cause, (II) compressing of the polymer 3D network structure which (III) deflects to the outer-velocity defect region and (IV) leaves the near-wall region exposed where the polymer molecules can undergo elongation.

CONCLUSION

Turbulent pipe flows containing polymer additives were measured in an experimental campaign during which over 122 experimental conditions with varying Reynolds number, polymer molecular weight and concentration were investigated. The maximum level of drag reduction observed was 72%. The outcome of the detailed analysis lies in the construction of universal trends of the dependency of the magnitude of the streamwise and spanwise rms velocity fluctuations and the Reynolds stresses, all at selected distances from the pipe wall, on the level of drag reduction. In addition, joint probability functions of streamwise and spanwise velocity fluctuations indicate that the polymer additives cause the turbulence to become increasingly anisotropic with polymer concentration. Finally, a new mechanism of polymer induced drag reduction in turbulent flow was proposed. This mechanism was based on the presence of physically entangled polymer molecules (i.e., 3D polymer network) in the vicinity of the wall, which would go some way towards explaining the appearance of a low-momentum flow region at this flow location.

REFERENCES

[1] Toms, B., *Proceedings to the International Congress on Rheology*, North-Holland, 1949

[2] Mysels, K.J., U.S. Pat. 2, 492,173 Dec 27 (1949)

[3] Berman, N., Drag reduction by polymers, *Annual Reviews Fluid Mechanics*, Vol. 10, 1978, pp. 47-64

[4] Brostow, W., Drag reduction in flow: review of applications, mechanism and predictions, *Journal of Industrial and Engineering Chemistry*, Vol. 14, 2008, pp. 409-416

[5] Liberatore, M., Baik, S., Mchugh, A. and Hanratty, T., Turbulent drag reduction of polyacrylamide solutions: effect of degradation on molecular weight distribution, *Journal of Non-Newtonian Fluid Mechanics*, Vol. 123, 2004, pp. 175-183

[6] Warholic, M., Heist, D., Katcher, M. and Hanratty, T., A study with Particle-Image Velocimetry of the influence of drag-reducing polymers on the structure of turbulence, *Experiments in Fluids*, Vol. 31, 2001, pp. 474-483

[7] Ptasinski, P., Nieuwstadt, F., Van den Brule, B. and Hulsen, M., Experiments in turbulent pipe flow with polymer additives at maximum drag reduction, *Flow, Turbulence and Combustion*, Vol. 66, 2001, pp. 159-182

[8] Warholic, M., Massah, H. and Hanratty, T., Influence of drag-reducing polymers on turbulence: effects of Reynolds number,

concentration and mixing, *Experiments in Fluids*, Vol. 27, 1999, pp. 461-472
[9] den Toonder, J., Hulsen, M., Kuiken, G. and Nieuwstadt, F., Drag reduction by polymer additives in a turbulent pipe flow: numerical and laboratory experiments, Journal of Fluid Mechanics, Vol. 337, 1997, pp. 193-231
[10] Zadrazil, I., Bismarck, A., Hewitt, G.F. and Markides, C.N., Shear layers in the turbulent pipe flow of drag reducing polymer solutions, *Chemical Engineering Science*, Vol. 72, 2012, pp. 142-154
[11] Morgan, R.G., Markides, C.N., Zadrazil, I. and Hewitt, G.F., Characteristics of horizontal liquid-liquid high-speed laser-induced fluorescence and particle velocimetry, *International Journal of Multiphase Flow*, Vol. 49, 2013, pp. 99-118
[12] White, C., Somandepalli, V. and Mungal, M., The turbulence structure of drag-reduced boundary layer flow, *Experiments in Fluids*, Vol. 36, 2004, pp. 62-69
[13] Ryskin, G., Turbulent drag reduction by polymers – a quantitative theory, Physical Review Letters, Vol. 59, 1987, pp. 2059-2062.
[14] Kalashnikov, V. and Tsiklauri, M., Supermolecular structures and flow birefringence in polymer solutions, Colloid and Polymer Science, Vol. 274, 1996, pp. 1119-1128